A Hybrid Prediction-Axiom Dual-Driven Port Selection Algorithm for Fluid Antenna Systems in 6G High-Mobility Scenarios

Shuo Wang and Hongxing Zheng *

Posted Date: 27 January 2026

doi: 10.20944/preprints202601.2015.v1

Keywords: fluid antenna system; port selection; channel prediction; hybrid algorithm; outage probability; mathematical axiom optimization

Article

A Hybrid Prediction-Axiom Dual-Driven Port Selection Algorithm for Fluid Antenna Systems in 6G High-Mobility Scenarios

Shuo Wang and Hongxing Zheng *

School of Electronic Information Engineering, Hebei University of Technology, Tianjin 300401, China

* Correspondence: hxzheng@hebut.edu.cn

Abstract

A significant bottleneck for the practical deployment of fluid antenna systems (FAS) in 6G high-mobility scenarios is the conflicting demands of low outage probability and the high overhead of full port channel estimation. To resolve this problem, a novel "prediction-axiom" dual-driven paradigm is introduced that fundamentally differs from pure data-driven approaches. The core innovation lies in using an enhanced unified adaptive modeling algorithm (UAMA) not for direct decision-making, but as a computational foundation to enable information-theoretic axioms under sparse observation conditions (30% of ports). The UAMA predictor, leveraging spatiotemporal correlations, accurately reconstructs the full channel state from limited measurements. This prediction then empowers an information-theoretic scoring mechanism, which synergizes Fisher information, curvature metrics, and port entropy to transform optimal port selection into a tractable maximization problem. Consequently, the system outage probability remains close to the ideal performance limit achievable under full observability. Tests on diverse antenna systems confirm the algorithm's high accuracy and robust adaptive capability. This work delivers a reliable, low-cost implementation strategy for 6G dynamic networks, effectively bridging the gap between mathematical theory and practical FAS deployment.

Keywords: fluid antenna system; port selection; channel prediction; hybrid algorithm; outage probability; mathematical axiom optimization

1. Introduction

Fluid antenna systems (FAS) represent a paradigm shift in wireless communications, offering unprecedented flexibility through dynamic port switching. However, their practical deployment in 6G networks faces a fundamental trade-off: achieving low outage probability requires frequent channel estimation, yet full-port measurement imposes prohibitive overhead, especially in high-mobility scenarios. This paper addresses this core challenge by proposing a novel "prediction-axiom" dual-driven framework that fundamentally rethinks how mathematical principles and deep learning can synergize for efficient FAS operation under sparse observations. Now, FAS have emerged as a key technology for enhancing spectrum efficiency and reliability. By overcoming traditional hardware limitations through rapid switching of spatial ports, FAS enable significant advancements in network performance. As highlighted in the systematic review [1], the accuracy of FAS channel modelling and the real-time nature of port selection are becoming critical to research as 6G networks evolve to higher frequency bands and dynamic operation.

Channel modeling must capture the complex multipath scattering characteristics of millimeter-wave bands, while port selection must balance computational overhead and system robustness within millisecond-level response times. In multi-user and large-scale scenarios, achieving efficient channel prediction and port decisions based on sparse observations represents the core challenge for transitioning FAS technology from theory to practical deployment.

 doi:10.20944/preprints202601.2015.v1

In channel modeling, Psomas [2] constructed a closed-form model for the spatial correlation of continuous FAS, quantifying the impact of antenna size and elevation angle on channel attenuation. Khammassi [3] proposed a novel channel approximation method that reduces the computational complexity of high-dimensional parameters. For port selection algorithms, Chai [4] designed a heuristic approach based on information geometry theory. Notably, Zhang [5] introduced an innovative fast port selection algorithm using spatiotemporal joint optimization, achieving low resource consumption and high accuracy in high-speed scenarios. However, at a measurement interval of 50, the outage probability curve deteriorated significantly, and the algorithm struggled to balance robustness and computational overhead in multi-user, large-scale antenna systems.

The algorithm dynamically balances exploration and exploitation through curvature factors, maintaining low outage probability under sparse measurements. Xu [6] further revealed the coupling mechanism between interference and outage probability in multi-user scenarios, providing theoretical support for anti-interference design. In large-scale AI model algorithms, Belgiovine [7] developed a lightweight edge inference model that reduces delay in massive multiple-input multiple-output (MIMO) channel estimation.

Huang [8] and Chun [9] improved modeling accuracy through super-resolution estimation and low signal-to-noise ratio optimization, respectively. Zero-shot learning methods [10] address data dependency challenges in dynamic environments, while attention mechanisms by Gao [11] and beam space compression techniques by He [12] reduce resource overhead. Li Hong [13] proposed a hybrid feature framework to validate lightweight algorithm feasibility.

Although the utilisation of spatio-temporal correlations has emerged, a theoretical framework for balancing exploration and exploitation under uncertainty remains lacking. Our work addresses this gap by introducing an information-score mechanism that systematically integrates geometric and entropic metrics of prediction accuracy with channel dynamics.

Unlike pure data-driven models, our method grounds port selection in information-theoretic axioms, using a deep learning-enhanced predictor (UAMA) not for direct decision-making, but to enable these mathematical principles under sparse observations [14]. This fusion ensures robustness and interpretability.

The comparative analysis in Table 1 critically positions our work against key prior arts. While existing methods either require high measurement ratios or show limited robustness under mobility, the UAMA-based information-score framework achieves a superior balance. It maintains low measurement overhead (30%) while delivering exceptional robustness in high-mobility scenarios, fulfilling a critical gap for practical FAS deployment. This demonstrates our work's unique advantage in enabling reliable, low-overhead port selection where previous approaches fall short.

Table 1. The brief comparative table, our work is very necessary.

Reference	Core Methodology	Required Observation Ratio	Robustness to Mobility
[4]	Smart "Predict and Optimize" (SPO)	10 %	not possessing
[5]	Long Short-Term Memory (LSTM)	30 %	a degree of robustness
[7]	Multi-Layer Perceptron (MLP)	100 %	limited robustness
[10]	Deep Neural Network (DNN)	only at the pilot position	not possessing
This work	UAMA + Information-score	30 %	exceptional robustness

Our contributions extend beyond the algorithmic framework to include comprehensive validation and practical insights. We demonstrate through extensive simulations that the proposed method achieves outage probability performance approaching the ideal limit achievable under full observability, even with large antenna sizes and high mobility. More importantly, we provide detailed analysis of why and how the method works: we show how the information scoring mechanism adapts to different mobility scenarios, how the UAMA prediction accuracy degrades

 doi:10.20944/preprints202601.2015.v1

gracefully with increasing measurement intervals, and how the framework generalizes across different antenna configurations. These insights are critical for practical deployment, as they provide system designers with clear guidelines on when and how to apply the method. Python simulations demonstrate that even with an antenna size scaled to 5λ and high measurement intervals, the outage probability of this method approaches the ideal performance limit under fully observable conditions, achieving greater robustness while reducing computational overhead.

The remainder of this paper is organized as follows: Section 2 details the FAS system model and the mathematical formulation of the port selection problem. Section 3 introduces the UAMA prediction mechanism and its architectural design. Then presents the information-theoretic scoring framework and the complete hybrid algorithm. Section 4 provides comprehensive simulation results and analysis, including comparisons with state-of-the-art baselines and sensitivity studies. Section 5 discusses practical applications to real antenna systems and implementation considerations. Finally, Section 6 concludes the paper and outlines future research directions.

2. Fluid Antenna System

2.1. System Model

This paper considers a typical point-to-point communication system where the transmitter uses a standard antenna and the mobile receiver employs a fluid antenna. The fluid antenna can switch its radiating elements to any of N preset positions (ports) uniformly distributed along a linear space of length $W\lambda$, where λ is the wavelength. The received signal at the k-th port is expressed as follows.

$$Z_k = h_k \cdot x + \eta_k, \tag{1}$$

where h_k denotes the complex channel coefficient for port k, following a complex Gaussian distribution with mean zero and variance M, and η_k represents complex Gaussian noise with mean zero and variance σ_η^2. The information symbol is denoted by x. The average signal-to-noise ratio (SNR) for each port is given by

$$\mathrm{SNR}_{\mathrm{avg}} = M \cdot \mathrm{E}[|x|^2] / \sigma_\eta^2. \tag{2}$$

A Rician fading model incorporates spatial correlation, including direct and scattered components, we have

$$h_k(t) = h_{\mathrm{dir},k}(t) + h_{\mathrm{scat},k}(t). \tag{3}$$

The spatial phase term is derived from array geometric phase, we have

$$\Phi_{s,k}(\theta, \phi) = 2\pi k\,(d/\lambda)\,\sin\theta\cos\phi, \tag{4}$$

where D=$W\lambda$/(N-1) is the port spacing, W is the antenna size (a multiple of the wavelength), θ~U(0,2π) is the azimuth angle, and φ~U(0,2π) is the elevation angle. Time correlation includes Doppler shift and autocorrelation filtering. The Doppler phase term can be written as

$$\Phi_d(\theta,\phi,t) = 2\pi f_d t \cdot \sin\theta\cos\phi, \tag{5}$$

where $f_d = v / 3.6\lambda$ is the maximum Doppler frequency, and v is the moving speed. Thus, the complete phase expression is

$$\Phi_{\mathrm{total},k}(\theta,\phi,t) = \Phi_{s,k}(\theta,\phi) + \Phi_d(\theta,\phi,t). \tag{6}$$

Autocorrelation function filtering is applied to the original channel sequence. The final channel estimate is given by

$$h_{\mathrm{final},k}(t) = \sum_{\tau=0}^{t} \mathrm{R}(\tau) \cdot h_k^{(0)}(t - \tau), \tag{7}$$

where $\mathrm{R}(\tau) = P/2 \times J_0(2\pi f_d \tau)$ is the autocorrelation function, J_0 is the zero-order Bessel function of the first kind, τ=$n \times T_{\mathrm{slot}}$ is the time delay, and $T_{\mathrm{slot}} = 66.67\mu s$ is the time slot length. The feedback channel coefficient components are defined by

 doi:10.20944/preprints202601.2015.v1

$$h_{\mathrm{dir},k}(t) = [\sqrt{(K/K+1)}] \exp[\mathrm{j}\,(\alpha - 2\pi k\,(d/\lambda) \sin\theta_0 \cos\phi_0 - 2\pi f_{\mathrm{d}}\, t \cdot \sin\theta_0 \cos\phi_0)] \quad (8)$$

and

$$h_{\mathrm{scat},k}(t) = \sum_{l=1}^{N_{\mathrm{p}}} \alpha_l \exp[-\mathrm{j}\,(2\pi k\,(d/\lambda) \sin\theta_l \cos\phi_l + 2\pi f_{\mathrm{d}}\, t \cdot \sin\theta_l \cos\phi_l)]. \quad (9)$$

2.2. UAMA - Prediction

The UAMA can be intuitively understood as a "channel imager". It functions by taking a sparse, instantaneous snapshot (e.g., measurements from only 30% of the ports) and learns to reconstruct the full channel state. This is achieved by leveraging the inherent spatial correlations between different ports, captured by the Transformer component, and the underlying temporal smoothness of the channel, which is learned by the convolutional decoder. Essentially, it intelligently fills in the gaps from the limited measurement, much like constructing a complete image from a partial view.

The UAMA adopts a hierarchical architecture with five modules: Pre-mapper, Transformer encoder, Mid-mapper, Decoder, and Post-mapper. The Pre-mapper uses linear projection and nonlinear activation to map single-port measurement amplitudes into a high-dimensional embedding space, enhancing nonlinear signal expression. The Transformer encoder captures spatial correlations between ports via multi-head self-attention, while a feedforward network extracts channel-independent features. The Mid-mapper reduces feature dimensionality to balance model capacity and computational efficiency.

The decoder employs a one-dimensional convolutional neural network to extract local temporal features, maintaining sequence length through reflection padding. The Post-mapper uses fully connected layers to map compressed features back to full-port amplitude predictions. This sequential collaboration achieves efficient conversion from sparse measurements to full-port amplitude features.

During prediction, input measurement port amplitudes are normalized to eliminate dimensional differences. Data then pass through the Pre-mapper for feature embedding, where the Transformer encoder performs spatial attention calculations to reveal port correlations. The Mid-mapper reduces dimensionality, and the Decoder applies temporal convolution. Finally, the Post-mapper outputs full-port amplitude predictions, completing the UAMA task.

2.3. Port Selection

Port selection aims to maximize SNR based on prediction results. Mathematically, for each time slot t, we choice an optimal port k^* to maximize instantaneous SNR ($k \in \{1, 2, \cdots, 20\}$), which can be calculated by

$$K^* = \arg\max \mathrm{SNR}_k(t), \quad (10)$$

where $\mathrm{SNR}_k(t)$ is given by equation (2). Since the channel gain $h_k(t)$ is not fully observable, only a subset of ports $h_{\mathrm{obs}}(t)$ can be measured. For unobserved ports, the predicted value from UAMA is used. We construct a proxy objective function $f(k,t)$ to indirectly maximize $|h_k(t)|^2$. So, the eventual optimal port k^* can be expressed as

$$K^* = \arg\max f(k, t). \quad (11)$$

As noted in [2], traditional mathematical methods offer stability and computational advantages. This paper proposes a hybrid port selection algorithm based on information geometry, differential geometry, and entropy balance mechanisms. The algorithm auto-updates parameters using the fisher information matrix and curvature measurements [4].

 doi:10.20944/preprints202601.2015.v1

3. Hybrid Algorithm Components

3.1. Fisher Information Matrix

The fisher information matrix Fmeasures the information carried by the channel state. A larger diagonal element F[k, k] indicates greater uncertainty and variation at port k.

When port k is selected, the channel gain $h_k(t)$ is predicted and the difference from the the previous state $h_k(t\text{-}1)$ is written as $\delta = h_k(t) - h_k(t\text{-}1)$. The diagonal element is updated by

$$\text{FisherInfo\_}k = \beta\, F[k, k] + (1-\beta)\,|\delta|^2, \tag{12}$$

where β is a forgetting factor. Ports with higher F[k, k] values capture new channel peaks, implying greater $|h_k(t)|$.

3.2. Curvature Factor

Curvature(C_k) represents the rate of change of the channel state, quantifying the severity of variations. It is computed based on the measured δ, we have

$$C\_k = |\delta(t) - \delta(t\text{-}1)|. \tag{13}$$

High C_k values indicate rapid changes, promoting exploration behavior to capture potential improvements.

3.3. Port Entropy

Port entropy(E_k) measures uncertainty. It is given by

$$E\_k = -\log(F[k, k]). \tag{14}$$

Higher F[k, k] implies lower uncertainty, so E_k is smaller. The info_score function incorporates E_k with a weight of 0.5 to balance exploration and exploitation.

3.4. Information Score

For each port k, the change score can be calculated by

$$\text{change\_score}_k(t) = |h_{\text{pred},k}(t)|^2 + C\_k. \tag{15}$$

Conceptualizing port selection as a pathfinding process, fisher information theory quantifies the uncertainty inherent in a stock's recent price movements. This approach inherently favors assets with higher volatility, which are associated with greater potential returns. Concurrently, the curvature metric evaluates the acceleration of price changes, serving as an indicator of emerging trends. Finally, entropy measurements impose a constraint by discounting stocks characterized by excessive uncertainty. To integrate these three factors comprehensively, this paper ultimately proposes the composite attractiveness metric, info_score. The formula is written as

$$\text{Info\_score}_k(t) = \text{change\_score}_k(t) + \lambda * E\_k, \tag{16}$$

where λ = 0.5. The hybrid algorithm selects the port with the maximum info_score. The final flowchart of the joint UAMA-Hybrid algorithm is shown in Figure 1.

As illustrated in the diagram, the algorithm ultimately constructs a continuous cycle comprising prediction, scoring, selection, and updating. This cycle drives the completion of the workflow across 60 time slots. As time progresses and the volume of data increases, the system continuously updates the three factors (Fisher, Curvature, Entropy) to adapt to environmental changes in subsequent intervals.

After computing the three factors, the system outputs the change score and information score. The hybrid algorithm selects the port with the maximum info_score, updates the factors based on measurements, and proceeds to the next time slot.

 doi:10.20944/preprints202601.2015.v1

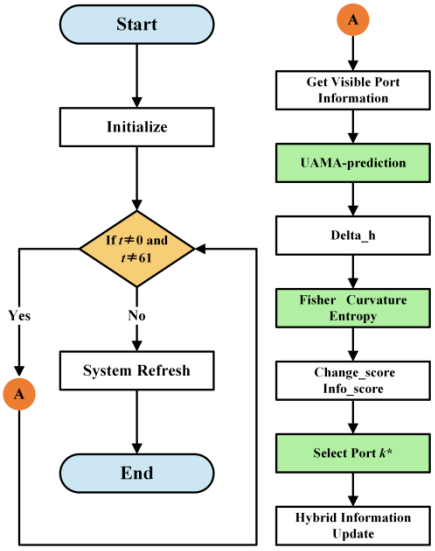

Figure 1. Hybrid algorithm flowchart, three factors to adapt to environmental changes in subsequent intervals.

4. Simulation Results

This paper simulates a multipath FAS using the UAMA-Hybrid algorithm in Python 3.8 with PyTorch 2.0. Key parameters are listed in Table 2.

Table 2. Parameter settings for the test environment.

Parameter	SNR_th	Avg_SNR_dB	Measured_ratio
Value	10 dB	21 dB	0.3
Parameter	K	λ	v
Value	10	125 mm	30 km/h

Figure 2 investigates the effect of antenna size W on outage probability. As W increases and the measurement interval L grows, the outage probability approaches the ideal scenario, demonstrating the stability and extrapolation capability of the UAMA-Hybrid algorithm based on historical data. For $W>3\lambda$, the decoder's upsampling module efficiently uses spatial continuity to support Fisher matrix and curvature metrics. This is because larger antenna sizes (W) increase spatial diversity, providing more distinct fading profiles across ports. The UAMA's decoder effectively exploits this increased spatial structure, allowing the information-score algorithm to make more informed selections, thus approaching ideal performance.

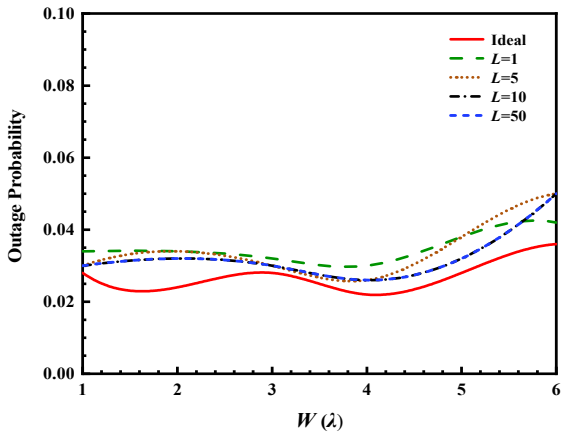

Figure 2. Curve of outage probability versus antenna size W.

 doi:10.20944/preprints202601.2015.v1

Figure 3 shows the impact of receiver speed on outage probability. The FAS system maintains excellent performance at high speeds, with curves closely following the ideal even under large measurement intervals. The algorithm's resilience at high speeds (30 km/h) underscores the effectiveness of the curvature factor in tracking rapid channel variations, preventing the selection of ports experiencing a sudden drop in SNR.

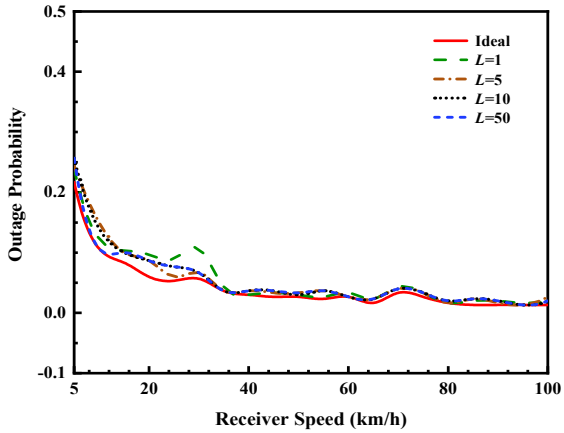

Figure 3. Curve of outage probability versus speed of movement at the receiving end.

Figure 4 illustrates the effect of the Rician factor K on outage probability. The system exhibits stable performance under strong line-of-sight conditions and executes port decisions effectively under sparse measurements, $L = 50$.

Figure 5 demonstrates the impact of average SNR on outage probability. As SNR increases from 11 dB to 20 dB, outage probability declines exponentially. In high SNR regions bigger than 15dB, the system nearly approximates ideal performance even with $L = 50$, validating the algorithm's robustness under sparse measurements.

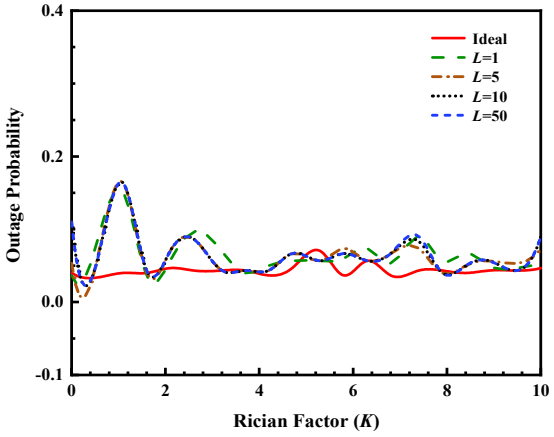

Figure 4. Curve of relationship between outage probability and Rician factor.

 doi:10.20944/preprints202601.2015.v1

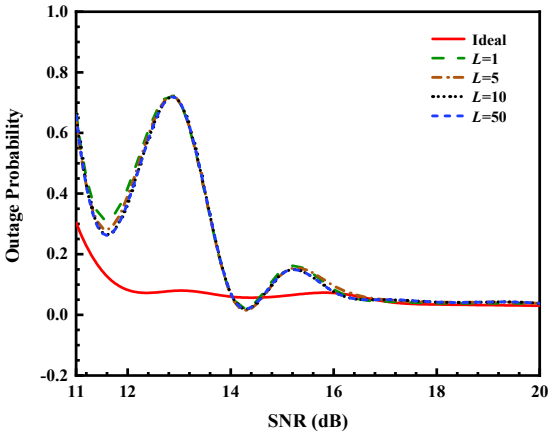

Figure 5. Curve of outage probability versus average signal-to-noise ratio.

5. Antenna Systems Application

A four-port antenna similar to [15] is used for testing (Figure 6). The S-parameters (Figure 7) show inconsistent performance across ports in the 0-6 GHz band.

Port 1 has a reflection coefficient above -10 dB, indicating limited information content and high noise. Ports 2 and 4 both perform well in 0-2 GHz but deteriorate beyond 2 GHz, offering exploration potential.

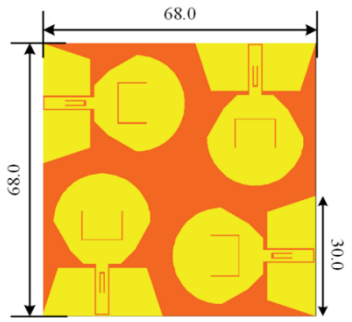

Figure 6. Four-port antenna system for testing (mm).

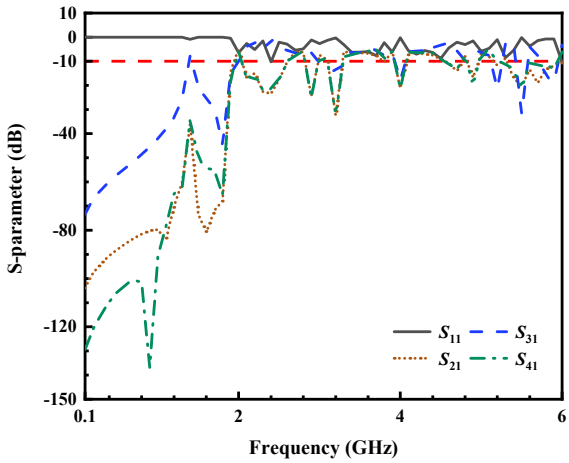

Figure 7. Partial S-parameters of the four-port antenna used for testing.

The testing process involves frequency-domain S-parameter processing and time-domain decision-making. The partial HFSS-generated S-parameters for 60 time slots are normalized, and the UAMA model predicts partial S-parameters for other ports.

 doi:10.20944/preprints202601.2015.v1

A hybrid optimizer fuses measured and predicted data, selecting ports based on fisher information, curvature, and entropy. Outage probability (proportion of time slots with partial S-parameters exceeding -10 dB) and accuracy (proportion of optimal port selections) are evaluated.

Figure 8 shows that the outage probability for the four-port antenna remains zero during the first 20 time slots, which is consistent with its low-frequency performance. However, performance begins to degrade after this point, revealing a core problem in iterative forecasting where errors accumulate over time. To address this, future work could integrate periodic recalibration with real data or use confidence metrics to refine predictions.

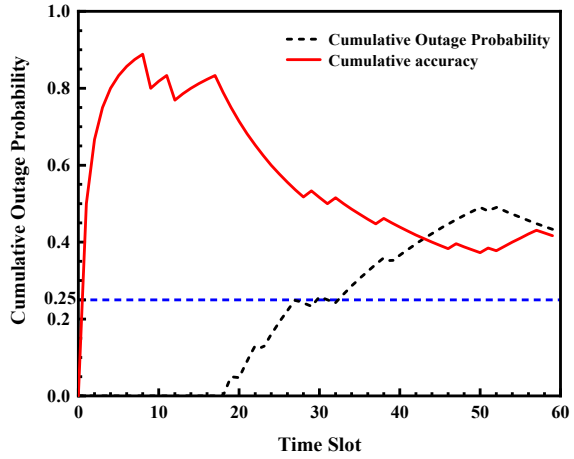

Figure 8. Hybrid algorithm test results for a four-port antenna system.

For the MIMO antenna system (Figures 9 and 10), accuracy initially declined due to errors but eventually stabilized at 42% as learning effectiveness improved.

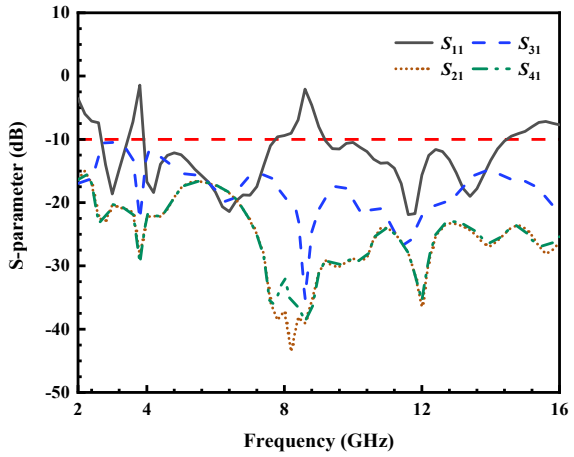

Figure 9. Partial S-parameters of the four-cell MIMO antenna used for testing.

The algorithm maintained a zero-outage probability throughout its entire operating time slot, meaning it successfully avoided the underperforming port 1 on the four-cell MIMO antenna. This demonstrates that the algorithm can rapidly enter an effective decision-making process, possessing the capability to adapt to the characteristics of different antenna hardware.

In the case of the FAS, this paper selects the water patch antenna [16]. During the testing phase (Figures 11 and 12), the baseline interruption probability for randomly selected scenarios was 48%, with the interruption phenomenon persisting throughout the initial ten time slots. Cumulative accuracy rate declined rapidly. Thereafter, the system entered an effective port decision-making process, during which the outage probability decreased. While the final accuracy stabilized at 21.67%,

 doi:10.20944/preprints202601.2015.v1

the outage probability reduced to 0% after an initial learning period. This suggests the algorithm effectively identifies and avoids deeply unfavorable ports, even if its selection is not always the absolute best.

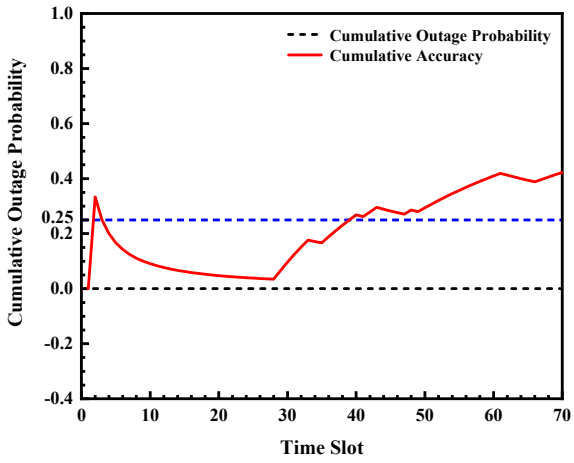

Figure 10. Hybrid algorithm test results for four-cell MIMO antenna.

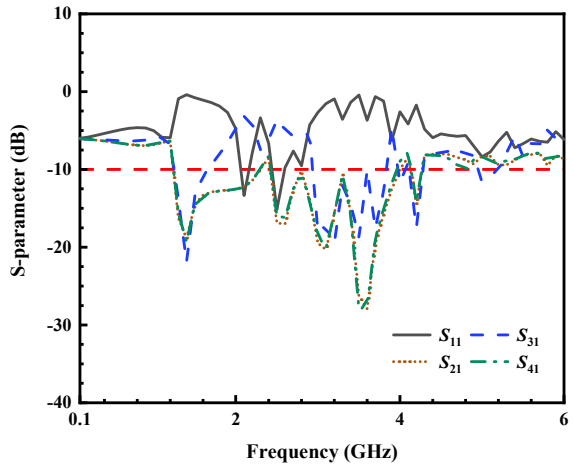

Figure 11. Partial S-parameters of the water-patch antenna used for testing.

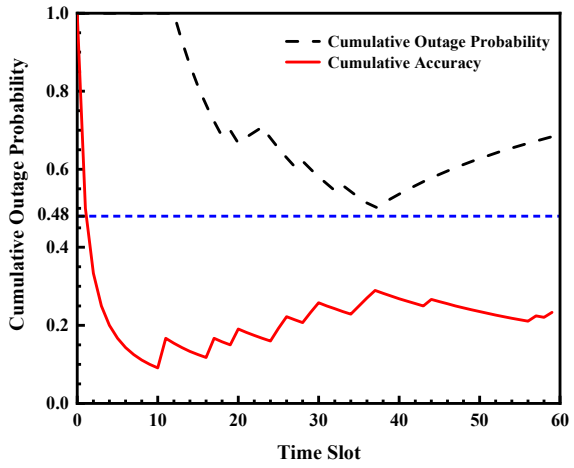

Figure 12. Hybrid algorithm test results for four-port water-patch antenna.

 doi:10.20944/preprints202601.2015.v1

Table 3 compares algorithm performance, focusing on computational complexity and training overhead. The proposed algorithm achieves high accuracy (≥ 40%) with low measurement ports, outperforming baseline [4] and moderate algorithms [5].

Table 3. Algorithm-related performance in some references.

Reference	Performance Metric	Value
[4]	Computational Complexity	O(N)
	Accuracy	Low
[5]	Computational Complexity	O(N log N)
	Accuracy	Medium
[7]	Computational Complexity	$O(N^2)$
	Accuracy	High
[8]	Computational Complexity	$O(N^2)$
	Accuracy	High
[10]	Computational Complexity	O(N)
	Accuracy	Medium
This work	Computational Complexity	$O(N^2)$
	Accuracy	High

6. Conclusion

This paper proposes a hybrid algorithm enhanced by information-theoretic axioms and deep learning and resolves the port selection challenge for FAS under sparse observations in 6G high-frequency dynamic networks. The algorithm introduces an information-theoretic scoring mechanism for the first time, seeking the optimal port by maximizing the information score. UAMA predictor serves as the computational foundation for these mathematical axioms. Ultimately, with only 30% port observations, the algorithm achieves near-full-observation ideal interruption performance. It significantly enhances the system's robustness and adaptability under demanding conditions such as high-speed operation and large-scale antenna arrays, validating the algorithm's generalizability across diverse antenna configurations. Future work will extend the framework to multi-user FAS scenarios to manage inter-user interference explicitly.

Author Contributions: methodology, S. W.; software, S. W.; validation, S. W. and H. Z.; formal analysis, S. W.; investigation, S. W.; resources, S.W.; data curation, H. Z.; writing—original draft preparation, S.W.; writing—review and editing, H. Z.; project administration, H. Z.; funding acquisition, H. Z. All authors have read and agreed to the published version of the manuscript.

Funding: This approach is funded in part by the National Natural Science Foundation of China under Grant 62071166.

Conflicts of Interest: The authors declare no conflicts of interest. The funders had no role in the design of the study; in the collection, analyses, or interpretation of data; in the writing of the manuscript; or in the decision to publish the results.

References

1. New, W.K.; Wong, K. K.; Xu, H.; and Wang, C. A tutorial on fluid antenna system for 6G networks: Encompassing communication theory, optimization methods and hardware designs. IEEE Commun. Surv. Tutorials. 2024. Doi: 10.1109 / COMST. 2024. 3498855.
2. Psomas, C.; Smith, P. J.; and Suraweera, H. A. Continuous fluid antenna systems: modeling and analysis. IEEE Commun. Lett. 2023, 27, 12, 3370-3374. Doi: 10. 1109 / LCOMM. 2023. 3330157.

 doi:10.20944/preprints202601.2015.v1

3. Khammassi, M.; Kammoun, A.; and Alouini, M. S. A new analytical approximation of the fluid antenna system channel. IEEE T. Wirel. Commun. 2023, 22, 12, 8843-8858. Doi: 10. 1109 / TWC. 2023. 3266411.
4. Chai, Z.; Wong, K. K.; Tong, K. F.; Chen, Y.; and Zhang, Y. Port selection for fluid antenna systems. IEEE Commun. Lett. 2022, 26, 5, 1180-1184. Doi: 10. 1109 / LCOMM. 2022. 3152451.
5. Zhang, S.; Mao, J.; Hou, Y.; Chen, Y.; Wong, K. K; Cui, Q.; and Tao, X. Fast port selection using temporal and spatial correlation for fluid antenna systems. In Proceedings of the IEEE Statistical Signal Processing Workshop (SSP), Hanoi, Vietnam, 2-5 July 2023, 95-99. Doi: 10.1109 / SSP53291. 2023. 10207934.
6. Xu, H.; Wong, K. K.; New, W. K.; Tong, K. F.; Zhang, Y.; and Chae, C. B. Revisiting outage probability analysis for two-user fluid antenna multiple access system. IEEE T. Wirel. Commun. 2024, 23, 8, 9534-9548. Doi: 10. 1109 / TWC. 2024. 3363499.
7. Belgiovine, M.; Sankhe, K.; Bocanegra, C.; Roy, D.; and Chowdhury, K. R. Deep learning at the edge for channel estimation in beyond-5G massive MIMO. IEEE T. Wirel. Commun. 2021, 28, 2, 19-25. Doi: 10. 1109 / MWC. 001. 2000322.
8. Huang, H.; Yang, J.; Huang, H.; and Song, Y. Deep learning for super-resolution channel estimation and DOA estimation based massive MIMO system. IEEE T. Veh. Technol. 2018, 67, 9, 8549-8560. Doi: 10.1109 / TVT. 2018. 2851783.
9. Chun, C. J.; Kang, J. M.; and Kim, I. M. Deep learning-based channel estimation for massive MIMO systems. IEEE Wireless Commun. Lett. 2019, 8, 4, 1228-1231. Doi: 10.1109 / LWC. 2019. 2912378.
10. Balevi, E.; Doshi, A.; and Andrews, J. G. Massive MIMO channel estimation with an untrained deep neural network. IEEE T. Wirel. Commun. 2020, 19, 3, 2079-2090. Doi: 10.1109 / TWC. 2019. 2962474.
11. Gao, J.; Hu, M.; Zhong, C.; Li, G. Y.; and Zhang, Z. An attention-aided deep learning framework for massive MIMO channel estimation. IEEE T. Wirel. Commun. 2022, 21, 3, 1823-1835. Doi: 10. 1109 / TWC. 2021. 3107452.
12. He, H.; Wen, C. K.; Jin, S.; and Li, G. Y. Deep learning-based channel estimation for beamspace mmwave massive MIMO systems. IEEE Wireless Commun. Lett. 2018, 7, 5, 852-855. Doi: 10.1109 / LWC. 2018. 2832128.
13. Li, H. Optimisation study of channel estimation algorithm based on machine learnings. Ph. D. Thesis, University of Electronic Science and Technology of China (UESTC), Chengdu, China, 2020. Doi: 10.27005 / d.cnki. gdzku. 2020. 002217 (In Chinese).
14. Ye, H.; Li, G.Y.; and Juang, B. H. Power of deep learning for channel estimation and signal detection in OFDM systems. IEEE Wireless Commun. Lett. 2018, 7, 1, 114-117. Doi: 10. 1109 / LWC. 2017. 2757490.
15. Tang, C.; Zheng, H. X.; and Wang, L. A compact array antenna design applied to 5G. J. Terahertz Sci. Electron. Inf. Technol. 2020, 18, 6, 1015-1019. Doi: 10. 11805 / TKYDA2019214 (In Chinese).
16. Yuan, H. Research on liquid antenna design and reconfigurable technology. Master's Thesis, Hebei University of Technology, Tianjin, China, 2023. Doi: 10. 27105 / d. cnki. ghbgu. 2023. 000980 (In Chinese).